PROCEEDINGS OF SPIE

SPIEDigitalLibrary.org/conference-proceedings-of-spie

Keck Planet Finder: design updates

Gibson, Steven, Howard, Andrew, Rider, Kodi, Roy, Arpita, Edelstein, Jerry, et al.

Steven R. Gibson, Andrew W. Howard, Kodi Rider, Arpita Roy, Jerry Edelstein, Marc Kassis, Jason Grillo, Sam Halverson, Martin M. Sirk, Christopher Smith, Steve Allen, Ashley Baker, Charles Beichman, Bruce Berriman, Thomas Brown, Kelleen Casey, Jason Chin, David Coutts, David Cowley, William Deich, Tobias Feger, Benjamin Fulton, Luke Gers, Yulia Gurevich, Yuzo Ishikawa, Ean James, Sharon Jelinsky, Stephen Kaye, Kyle Lanclos, Adela Li, Scott Lilley, Ben McCarney, Tim Miller, Steve Milner, Timothy J. O'Hanlon, Jacob Pember, Mike Raffanti, Constance Rockosi, Ryan Rubenzahl, Dave Rumph, Dale Sandford, Maureen Savage, Christian Schwab, Andreas Seifahrt, Abby Shaum, Roger Smith, Julian Stuermer, Jim Thorne, Adam Vandenberg, Tod Von Boeckmann, Cindy Wang, Qifan Wang, Marie Weisfeiler, Mavourneen Wilcox, Edward H. Wishnow, Peter Wizinowich, Truman Wold, Anna Wolfenberger, "Keck Planet Finder: design updates," Proc. SPIE 11447, Ground-based and Airborne Instrumentation for Astronomy VIII, 1144742 (13 December 2020); doi: 10.1117/12.2561783

SPIE.

Event: SPIE Astronomical Telescopes + Instrumentation, 2020, Online Only

Downloaded From: https://www.spiedigitallibrary.org/conference-proceedings-of-spie on 02 May 2021 Terms of Use: https://www.spiedigitallibrary.org/terms-of-use

Keck Planet Finder: Design Updates

Steven R. Gibson[a], Andrew W. Howard[b,a], Kodi Rider[a], Arpita Roy[c], Jerry Edelstein[a], Marc Kassis[d], Jason Grillo[a], Sam Halverson[e], Martin M. Sirk[a], Christopher Smith[a], Steve Allen[f], Ashley Baker[b,*], Charles Beichman[g], Bruce Berriman[g], Thomas Brown[d], Kelleen Casey[d], Jason Chin[d], David Coutts[h], David Cowley[f], William Deich[f], Tobias Feger[h], Benjamin Fulton[g], Luke Gers[d], Yulia Gurevich[h], Yuzo Ishikawa[i], Ean James[d], Sharon Jelinsky[a], Stephen Kaye[b], Kyle Lanclos[d], Adela Li[a], Scott Lilley[d], Ben McCarney[d], Tim Miller[a], Steve Milner[d], Timothy J. O'Hanlon[a], Jacob Pember[h], Mike Raffanti[a], Constance Rockosi[f,j], Ryan Rubenzahl[b], Dave Rumph[b], Dale Sandford[f], Maureen Savage[f], Christian Schwab[h], Andreas Seifahrt[k], Abby Shaum[g], Roger Smith[b], Julian Stuermer[l], Jim Thorne[d], Adam Vandenberg[d], Tod Von Boeckmann[d], Cindy Wang[g], Qifan Wang[b], Marie Weisfeiler[a,m], Mavourneen Wilcox[d], Edward H. Wishnow[a], Peter Wizinowich[d], Truman Wold[d], and Anna Wolfenberger[a]

[a]Space Sciences Laboratory, University of California, Berkeley, United States
[b]California Institute of Technology, Pasadena, United States
[c]Space Telescope Science Institute, Baltimore, United States
[d]W. M. Keck Observatory, Kamuela, United States
[e]Jet Propulsion Laboratory, California Institute of Technology, Pasadena, United States
[f]University of California Observatories, Santa Cruz, United States
[g]IPAC-NASA Exoplanet Science Institute, Pasadena, United States
[h]Macquarie University, Sydney, Australia
[i]Johns Hopkins University, Baltimore, United States
[j]University of California, Santa Cruz, United States
[k]University of Chicago, Chicago, United States
[l]Heidelberg University, Heidelberg, Germany
[m]Columbia Law School, New York, United States
[*]51 Pegasi b Fellow

ABSTRACT

The Keck Planet Finder (KPF) is a fiber-fed, high-resolution, high-stability spectrometer in development at the UC Berkeley Space Sciences Laboratory for the W.M. Keck Observatory. KPF is designed to characterize exoplanets via Doppler spectroscopy with a goal of a single measurement precision of $0.3\,\mathrm{m\,s^{-1}}$ or better, however its resolution and stability will enable a wide variety of astrophysical pursuits. Here we provide post-preliminary design review design updates for several subsystems, including: the main spectrometer, the fabrication of the Zerodur optical bench; the data reduction pipeline; fiber agitator; fiber cable design; fiber scrambler; VPH testing results and the exposure meter.

Keywords: Spectrometer, exoplanets, Doppler spectroscopy, radial velocity, Zerodur

Corresponding author email: sgibson@ssl.berkeley.edu

Ground-based and Airborne Instrumentation for Astronomy VIII, edited by Christopher J. Evans,
Julia J. Bryant, Kentaro Motohara, Proc. of SPIE Vol. 11447, 1144742 · © 2020
SPIE · CCC code: 0277-786X/20/$21 · doi: 10.1117/12.2561783

Downloaded From: https://www.spiedigitallibrary.org/conference-proceedings-of-spie on 02 May 2021
Terms of Use: https://www.spiedigitallibrary.org/terms-of-use

1. INTRODUCTION

The Keck Planet Finder (KPF) is a fiber-fed, high-resolution, high-stability spectrometer in development for the W.M. Keck Observatory (WMKO). The instrument is designed to characterize exoplanets via Doppler spectroscopy with a goal of a single measurement precision of $0.3\,\mathrm{m\,s^{-1}}$ or better; however, its resolution and stability will enable a wide variety of other astrophysical pursuits. KPF will cover a wavelength range of 445 nm to 870 nm over green and red channels. A unique aspect of KPF is the use of a Zerodur optical bench to support the spectrometer optics. Zerodur is a high-stability, glass-ceramic material with a near-zero response to temperature, and was chosen to provide instrumental stability against temperature changes. A schematic overview of the KPF system is shown in Figure 1.

Several institutions contribute to the KPF project: the Space Sciences Laboratory (SSL) at UC Berkeley is the primary design and build location; the California Institute of Technology (Caltech) is the science center for KPF, is developing the data reduction pipeline and, is also involved with the design and testing of the detectors; WMKO is responsible for the fiber injection unit (FIU), facility modifications, and instrument software; University of California Observatories (UCO) is working on detector design and characterization as well as instrument software; and Macquarie University is developing the Fabry-Pérot etalon for the KPF calibration system.

The design period since our 2018 KPF SPIE paper[1] has been one of refinement, without large departures from the overall instrument design presented at that time. As such, the reader is referred back to our 2018 paper for a more complete overview of the entire KPF instrument.

We note here two recent additions to the KPF system:

- **Laser Frequency Comb:** To expand upon our suite of available calibration sources, we have added a broadband laser frequency comb (LFC) from Menlo Systems. The LFC will serve as the primary wavelength calibration source, providing stable, uniformly-spaced emission lines across the KPF bandpass that are traced to a fundamental frequency standard that is stable at the 10^{-14} level.[2]

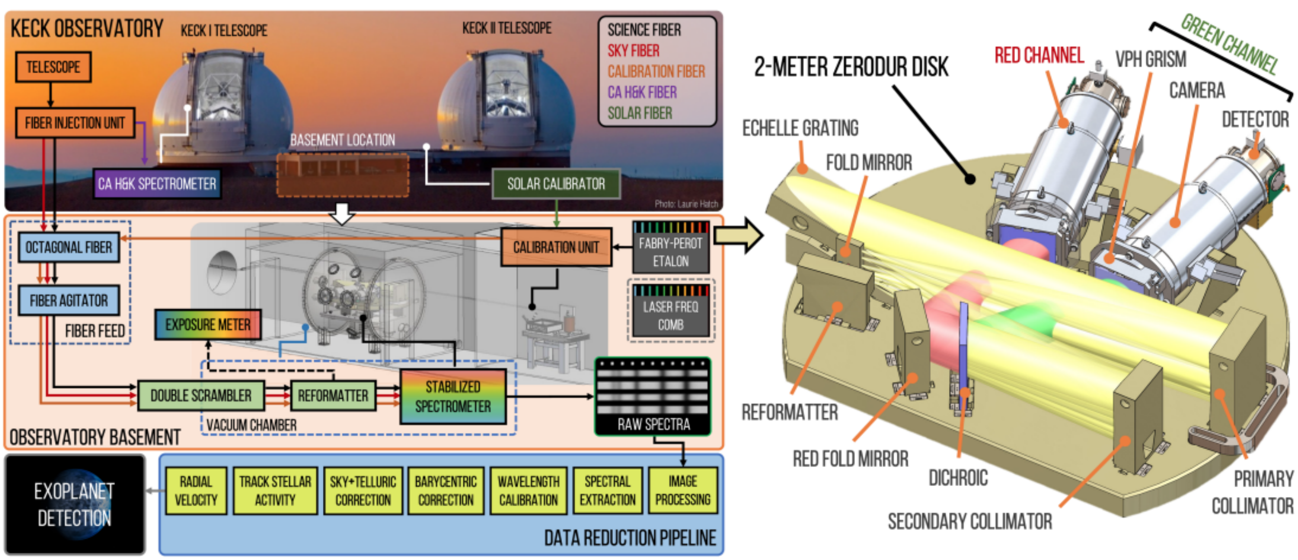

Figure 1. The KPF instrument, spanning subsystems from the telescope fiber injection unit to the data reduction pipeline (left), each optimized for precision and efficiency. At the core is an asymmetric white-pupil spectrometer (right) on a Zerodur bench with Zerodur mounts and optics for maximum stability, enclosed within a thermally-controlled vacuum chamber.

Downloaded From: https://www.spiedigitallibrary.org/conference-proceedings-of-spie on 02 May 2021
Terms of Use: https://www.spiedigitallibrary.org/terms-of-use

- **Solar Calibrator:** A dedicated solar monitoring system has been added, which will feed KPF with stable, disc-integrated sunlight throughout the day. This 'sun-as-a-star' dataset will be important for assessing the performance of the instrument and analysis techniques, and for gaining insight into the lowest-level activity signals across a wide range of timescales.[3] We anticipate using the solar calibrator to assess Doppler precision and instrument stability during testing at SSL and commissioning in Hawaii.

The majority of KPF subsystems are currently undergoing final fabrication or assembly, as summarized within Figure 2. Assembly of the main spectrometer will begin in early 2021.

Within this paper, we present updates and details on several subsystems within KPF, including: the main spectrometer, the fabrication of the Zerodur optical bench; the data reduction pipeline; fiber agitator; fiber cable design; fiber scrambler; VPH testing results and the exposure meter.

2. MAIN SPECTROMETER

For cross-dispersion, the KPF main spectrometer utilizes a grism (*gr*ating-pr*ism*) within each of the green and red arms. Within the grisms, the primary dispersing elements are volume phase holographic (VPH) gratings. A prism bonded to the front of each VPH grating provides the advantage of introducing beam anamorphosism in the cross-dispersion direction.

At the time of the 2018 KPF paper, the prism glass type was Ohara S-FSL5Y. This was chosen from a stability standpoint, as it exhibits a near-zero index of refraction change with temperature (dn/dT ~ 0). However, a closer look at the grism bonding process revealed that S-FSL5Y has a coefficient of thermal expansion (CTE) 17.5x higher than the fused silica substrates of the VPH gratings. Given the large CTE change across the prism-VPH bond line, there was concern of damage caused by differential expansion with temperature changes (especially during shipping).

As such we undertook a trade study to find a prism glass type that offered a lower CTE and also exhibited high thermal stability within the instrument. Based on this trade study we chose fused silica for both the green and red prisms, which our analysis showed offered acceptable thermal stability and also removed the differential-CTE concerns entirely.

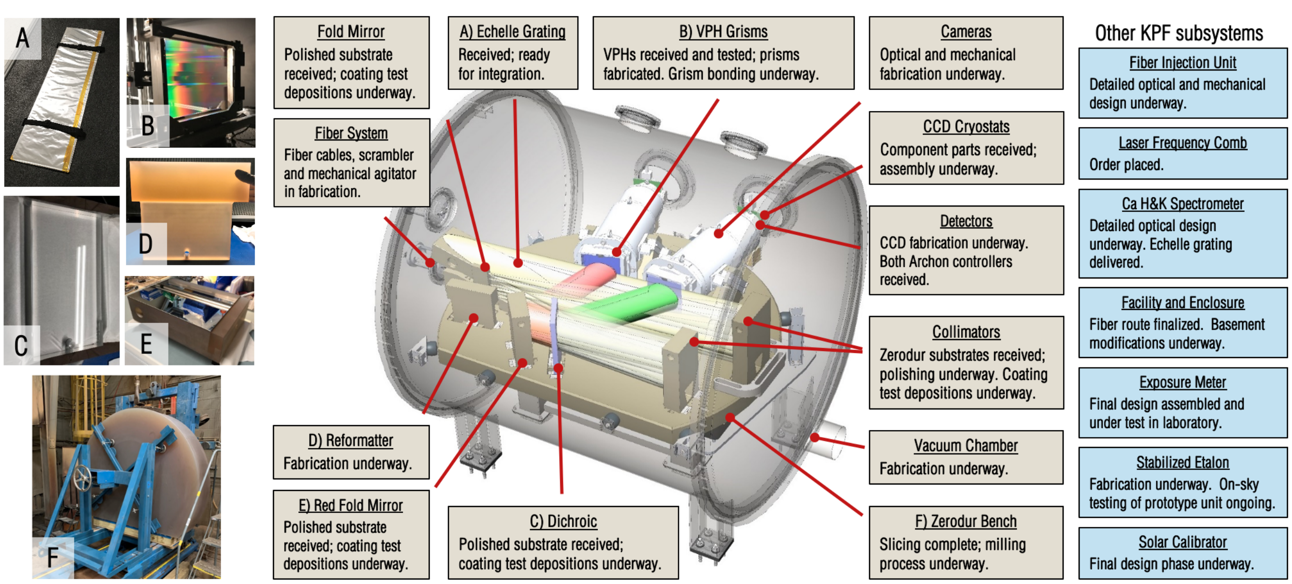

Figure 2. Overview of the development status of KPF components and subsystems.

Downloaded From: https://www.spiedigitallibrary.org/conference-proceedings-of-spie on 02 May 2021
Terms of Use: https://www.spiedigitallibrary.org/terms-of-use

3. FABRICATION OF THE ZERODUR OPTICAL BENCH

KPF is unique in its extensive use of Zerodur, a very low CTE material, to achieve the high thermal mechanical stability required in precision radial velocity (PRV) spectrometers. The optical bench, reformatter, collimators, echelle, fold mirrors, and camera mounts are all made of Zerodur. Since completing our preliminary design review (PDR) all of these elements have entered production.

3.1 Preliminary Zerodur Processing

The KPF Zerodur is mostly sourced from a large 2 m diameter by 0.4 m disk of Zerodur Extreme remaining from a previous mission at SSL. This disk was processed into blanks at the Corning Incorporated Canton facility in Canton, NY, as shown in Figure 3.

The disk was first sliced into separate pieces. The initial cut, parallel to the disk axis, (which we call the "D-cut"), produced a large full depth piece from which we could obtain several of our optic blanks. The remaining disk was then cut into three roughly equal slices. The bottom slice was chosen to become our primary bench blank and has been shipped to Schott AG in Mainz Germany for final machining. The top slice is our backup bench blank which can be used if any issues are encountered during manufacturing or shipping of the primary bench. The middle slice was used to provide the primary and backup blank for the primary collimator, with the remainder available for other backup material should we need it.

The D-cut was further processed to remove material for the echelle mount, secondary collimator, reformatter base and the fold mirror. These were cut, machined, and ground at Corning into the rough-cut blanks for these parts. The blanks were then shipped to Advanced Glass Industries, Mindrum Precision, Precision Asphere, and Winlight Systems for final milling and polishing. The echelle base material will be shipped to Schott for final milling.

3.2 Acid Etching of the Bench

In our preliminary design review and subsequent manufacturing readiness review it was suggested that we acid etch the bench after milling. It had always been a project desire to acid etch the bench to reduce risk but we had decided not to pursue it because our low levels of stress (<10 MPa) implied it was not necessary. It was also technically challenging to accomplish on such a large disk. However, comments from our reviewers caused us to take a closer look to see what could be done. Corning has a large tank that could acid etch the entire disk in one operation. However they have not previously etched Zerodur and had no experience using the particular acid etching formula for Zerodur, a mixture of 2 parts Hydrofluoric and 1 part Hydrochloric acid. For a bench ground with D64 tool (with bonded diamond grains per DIN 848) we would need to etch the optical bench for approximately 30 minutes to remove the right amount of material. At this etch rate it was going to be difficult to remove the acid from such a large tank and properly rinse the bench in time to guarantee uniform etch rates. In

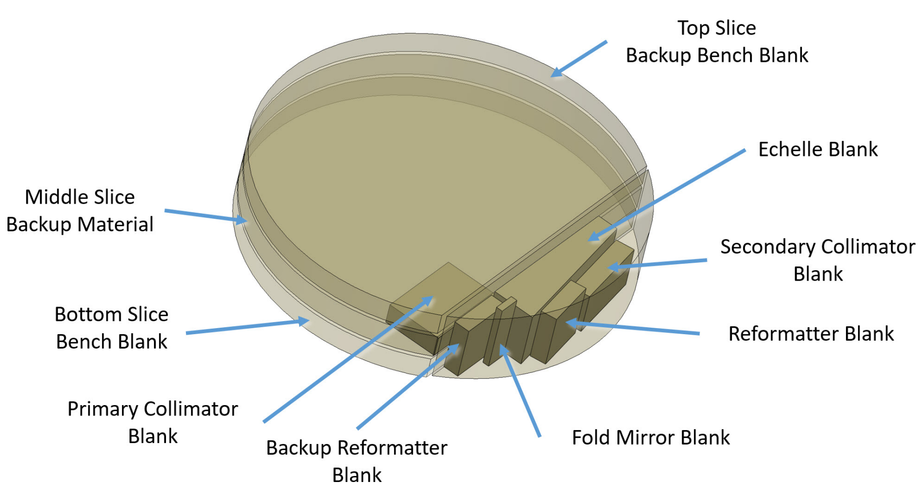

Figure 3. Plan for slicing the KPF Zerodur blank into component parts.

Downloaded From: https://www.spiedigitallibrary.org/conference-proceedings-of-spie on 02 May 2021
Terms of Use: https://www.spiedigitallibrary.org/terms-of-use

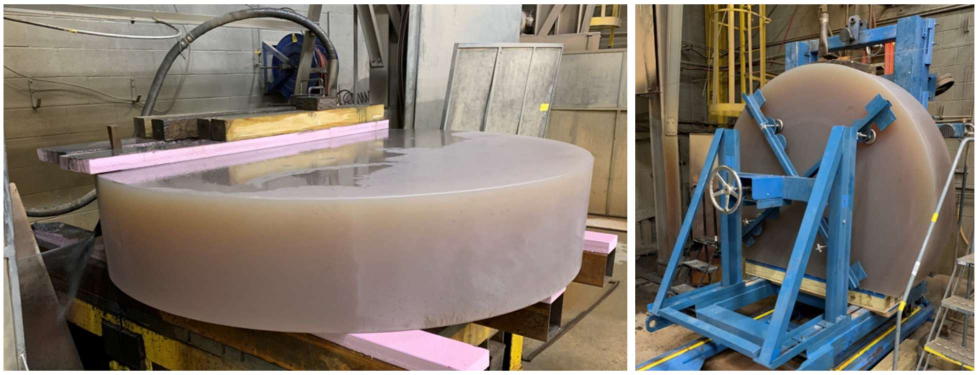

Figure 4. Zerodur blank processing at Corning. Left: D-Cut wire saw slicing. Right: Top wire saw slice removal.

addition, there was concern that acid at the etching interface would refresh at different rates at different pocket depths. At the top there would be good access to a large reservoir of active acid but at the bottom of the pockets access to fresh etchant may have been slower. If true, this would produce different material removal vs. depth in the pockets which was undesirable. See Figure 5 for an example pocket geometry that would need to be etched.

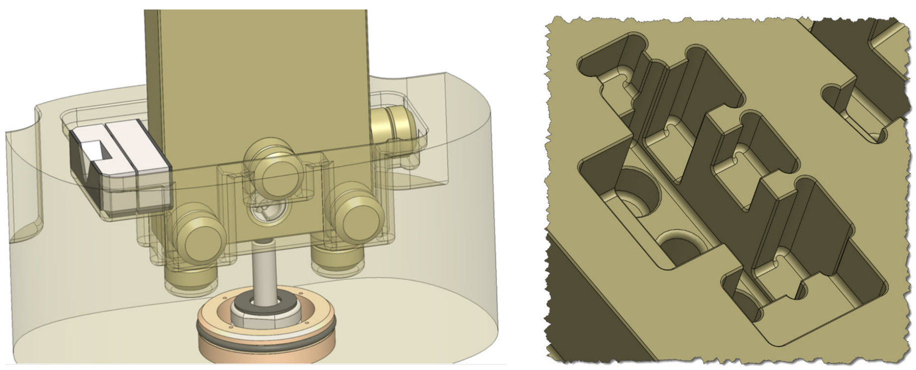

Figure 5. Two views of the fold mirror mounting pocket in the optical bench.

Schott does not have a tank of their own large enough to process our bench but have subcontractors that regularly process large Zerodur pieces. At both Corning and the Schott subcontractors the price for acid etching the entire bench was beyond the resources of this project.

Ammonium Bifluoride can also be used to etch Zerodur. It has a much lower etch rate (0.43 micron/min) than Hydrofluoric/Hydrochloric acid (HF-HCL) (3.1 micron/min).[4] When used as a paste, Ammonium Bifluoride will exhaust its reaction after approximately 30 min. For each application of Ammonium Bifluoride paste it will etch approximately 13 micron of Zerodur in 30 minutes. At a D64 grind we would need to apply Ammonium Bifluoride five or six times to remove the minimum material. At a finer D46 grind we would need to etch four or five times to remove the minimum material. Due to the input from our reviewers and the investigations outlined above we have decided to etch just the higher stress regions of the bench with multiple applications of Ammonium Bifluoride paste. The pockets will be ground to the finer level of D46 at Schott in Mainz, Germany and we will make use of the extensive expertise of Dennis McBride and his team at WMKO to etch the pockets in-house at SSL.

Downloaded From: https://www.spiedigitallibrary.org/conference-proceedings-of-spie on 02 May 2021
Terms of Use: https://www.spiedigitallibrary.org/terms-of-use

4. DATA REDUCTION PIPELINE

As a profusion of precision spectrographs prepare for commissioning and science operations,[5] the uniform and comprehensive processing of complex echelle data remains a common challenge within the ground-based radial velocity (RV) community. In the KPF development plan, we recognize this seminal role of the data reduction pipeline (DRP), and treat it as a full instrument sub-system with its own management structure, dedicated team, and independent reviews. Within the larger schedule, software and hardware are being developed and tested in tandem — a practice that will hopefully stand us in good stead during AI&T and into commissioning.

The team of astronomers and software engineers working on the KPF DRP are attempting to produce truly industry-standard code, inculcating best practices like rigorous version control, modular development, and in-built regression-performance-verification testing. To ensure scientific performance and precision delivery, we are drawing on the best available algorithms collected across instrument teams while budgeting time for areas that will need innovation. This DRP is conceptualized from the beginning to be flexible and applicable to other instruments, and for modular community-based development in the future. While its primary role is to deliver high-quality processed data for KPF, we have always planned to make the DRP available to the larger community for sophisticated cross-instrument analysis. An important point to note is that the currently scoped DRP will not correct for stellar activity effects, although it will deliver various activity metrics (bisector inverse slope, canonical line indicators etc.) since this is still an open area of research in exoplanet and stellar science. However, the modular nature of the DRP leaves open the possibility for publicly contributed solutions that can be easily made available within the workflow to users in the future.

The KPF DRP functions within the Keck Data Reduction Pipeline Framework, which is a lightweight software ecosystem created to unify the processing of data from various instruments at WMKO. Data products generated by the pipeline will also be fully integrated and compliant with the Keck Observatory Archive (KOA) maintained by the NASA Exoplanet Science Institute (NExScI). Currently our DRP is still in modular testing phase with a simple version of essential steps implemented to ensure basic end-to-end execution on spectra from multiple instruments (e.g. HARPS, NEID, PARAS). We have recently completed two reviews; an external Pipeline Architecture Design Review, and an internal Data Model Readiness Review. In terms of schedule, we are on track to deliver Version 1 of the DRP to the larger KPF team in January 2021, ahead of instrument assembly and the first acquisition of detector reads. We plan to deliver Version 2 in early 2022, ahead of commissioning, with all modules in place and tested on laboratory data from the instrument. Finally, Version 3 will be delivered in late 2022, once real on-sky data from the instrument at the telescope allows us to bring all modules to the level of sophistication necessary to reach the precision goals of KPF.

5. FIBER AGITATOR

5.1 Agitator Design

During our preliminary design phase, we designed and built a fiber agitator based on the system described in Roy et al. (2014).[6] This mechanism employed two reciprocating linear stages to change the shape of the fiber path, which follows a stylized "W". The performance of this design was presented in detail by Sirk et al. (2018),[7] and while yielding excellent results we later discovered that the majority of modal noise reduction was occurring not within the agitator, but rather outside it along a freely hanging length of fiber in which the agitator was inducing vibrations. Subsequent tests done by hand showed that excellent performance is achieved with small amplitude ($\sim 2-3$ cm) motions at around 2 Hz on sections of fiber that are free to move. We decided to build a new mechanism that mimics the quasi-chaotic and gently percussive motion of hand-agitation.

The newly designed KPF prototype agitator utilizes a Galil brushless motor to which is attached a 3-inch diameter wheel. Perpendicular to the wheel at a radius of 1 inch are attached two steel rods supporting freely turning PTFE bushings. The fiber is inserted into a length of Miniflex PBT tubing (5 mm OD, 3 mm ID) which is then coiled into two unequally sized loops and suspended vertically above the bushings. When the motor is turned, the two bushings alternately tap the PBT tubing and induce vibrations that change the shape of the coils. Figure 6 shows our agitator prototype in operation.

Downloaded From: https://www.spiedigitallibrary.org/conference-proceedings-of-spie on 02 May 2021
Terms of Use: https://www.spiedigitallibrary.org/terms-of-use

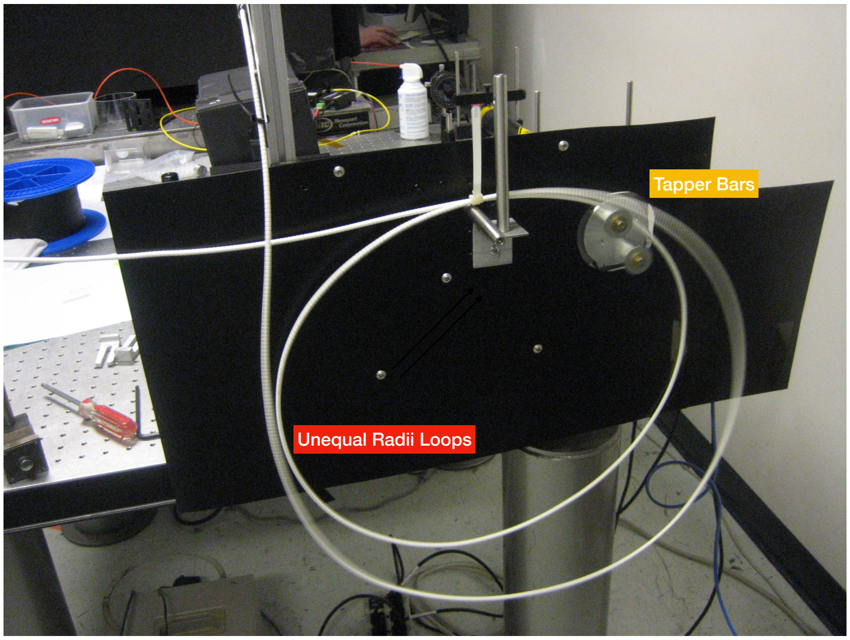

Figure 6. The KPF 2-coil fiber agitator prototype in operation at ∼2 Hz. Blurring of PBT tubing gives a sense of size of oscillations.

5.2 Agitator Optical and Mechanical Performance

The agitator has three parameters which can be adjusted: the diameter of the fiber loops, the radius of the tapper-bars, and the motor frequency. Early tests indicated that fiber loops 30 to 40 cm in diameter showed excellent modal noise reduction, and that tapper-bars at 1 inch radius imparted the necessary motion of the fiber loops. The prototype motor was controlled by a custom Python program that allowed adjustment of the rotation frequency.

To measure agitator performance we injected coherent 543 nm HeNe laser light into one end of a 16 m, 200 μm core octagonal fiber and imaged the other end with a microscope. These images were evaluated for signal-to-noise[8] (smoothness) and for image centroid stability, and were compared to similar images obtained with a broadband green LED (FWHM = 35 nm) which shows no modal noise.

Sets of 30 exposure were obtained at various exposure times and motor frequencies. Figure 7 shows the signal-to-noise ratio (S/N) for a range of motor frequencies obtained in 2 second exposures. Also plotted is a case where the agitator was off, a case where agitation was induced by hand, and a case where the illumination was by the broadband LED.

These data sets were also analyzed for near-field image centroid stability, which was then translated into an equivalent radial velocity (as an estimate of what would be seen by the KPF spectrometer). For each test, the image centroid of the fiber core was determined for the 30 images and the RMS determined. Figure 8 plots image stability as a function of exposure time for several different motor frequencies, and for hand agitation.

In addition to reducing modal noise the agitator must also not induce focal ratio degradation (FRD) while in operation, as well as over time. To verify long-term stability we performed a life test in two phases. In Phase I the agitator was run at 1.9 Hz for a month (5 million cycles, equating to 4 months of the agitator in use within KPF). We periodically measured FRD by analyzing output ring widths using input collimated light. When run at this frequency the agitator induces no FRD. At the end of the first month FRD was also measured using full-cone (f/3.7) light. Phase II was performed at an accelerated rate of 16 Hz with the tapper bars set at 1/2-inch radius. This test was run continuously for seven weeks (105 million cycles, or simulating 6.6 years of use with KPF). FRD was measured with collimated and full-cone light as per Phase I. No changes in collimated light ring width, or full-cone f/# was observed. At the end of Phase II the fiber was removed from the PBT tubing and inspected for wear and damage. A slight dulling of the polyimide coating was noticed at the location

Downloaded From: https://www.spiedigitallibrary.org/conference-proceedings-of-spie on 02 May 2021
Terms of Use: https://www.spiedigitallibrary.org/terms-of-use

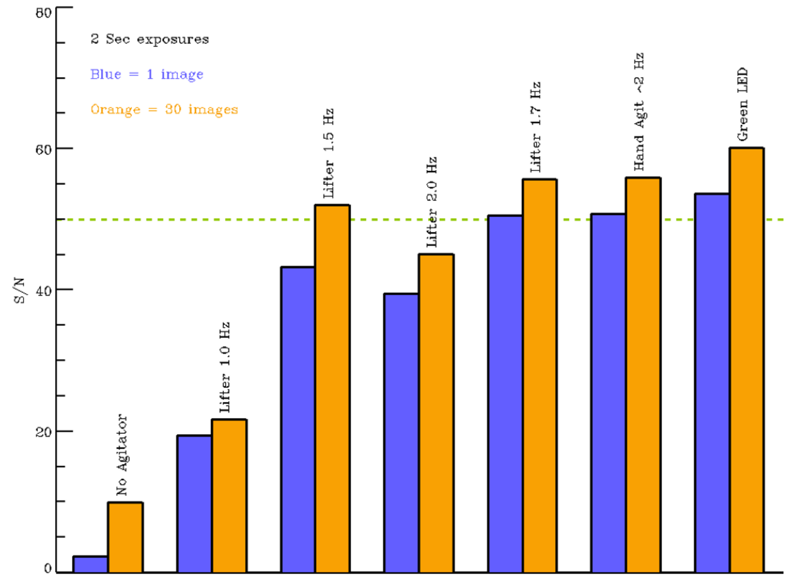

Figure 7. Agitator comparisons. The term 'Lifter' here refers to the 2-coil agitator design shown in Figure 6. Blue bars are S/N for a single 2 s exposure, orange bars show the the S/N for averages of 30 exposures. At 1.7 Hz modal noise is reduced to levels comparable to hand agitation and the green LED in just 2 seconds.

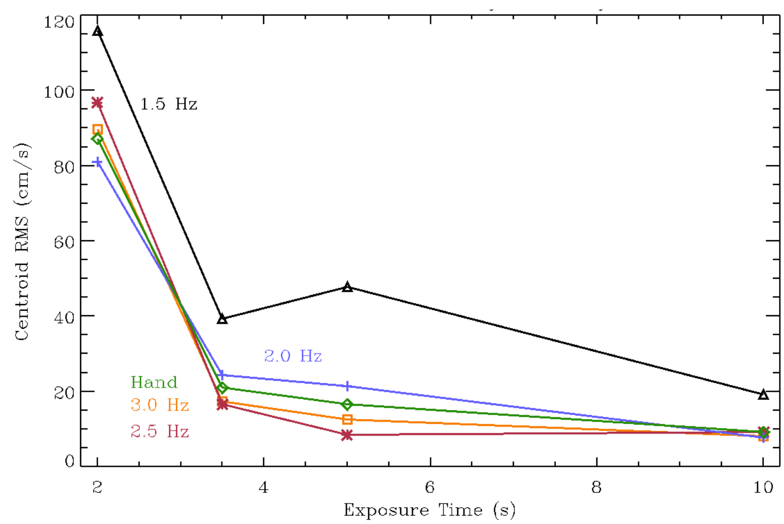

Figure 8. Agitator image centroid scatter *vs.* exposure time for different motor frequencies. For frequencies >∼1.5 Hz velocity scatter is reduced to levels comparable to hand agitation in under 4 seconds.

along the fiber where the tapper bars struck the PBT tubing. Laser light was injected into the input end and the entire length inspected for light leaks. None were observed. After the eleven weeks of continuous operation the outer PBT protective tubing showed about 0.2 mm of wear at the tapper bar impact point. This was mitigated by a single layer of Kapton tape.

The 2-coil KPF agitator prototype met all its design requirements at the expense of only 2.5 m of fiber. The design employs very few moving parts, is easily serviced, and does not damage the fiber. Modal noise is reduced to levels comparable to broadband light in under 4 seconds. Full details of the the new KPF agitator are forthcoming.[9]

Downloaded From: https://www.spiedigitallibrary.org/conference-proceedings-of-spie on 02 May 2021
Terms of Use: https://www.spiedigitallibrary.org/terms-of-use

6. FIBER CABLE DESIGN

6.1 Fiber Strain Relief

Several optical fibers carry light between the Fiber Injection Unit (FIU) within the AO room on the Keck I telescope and the the observatory basement where the majority of the KPF subsystems reside. Each optical fiber will be protected along this route within flexible, hard-plastic tubing (Miniflex PBT). These fiber cables will be also be placed inside covered trays along the route to add an extra layer of protection from every-day observatory activities. Fibers longer than ~ 25 meters, described as "long fibers" hereafter, contain a Strain Relief Box (SRB) to decouple the optical fiber from its Miniflex PBT tubing due to the thermal coefficient mismatch of the two materials. The SRB was originally designed in a long, rectangular shape; however, the 1.2 meter capacity requirement led to infeasible dimensions for our mounting application. Instead, the SRB layout changed to a circular geometry to take advantage of the circumference of a circle, which grows by a factor of π and therefore has a more efficient packing factor. The SRB contains an inner circle to enforce the 10 cm minimum bend radius of our fibers and an outer circular racetrack to constrain the maximum capacity. Flattened dovetail racetrack grooves were milled at each wall to prevent the fiber from slipping over the wall. The Miniflex tubing attaches to the SRB with two Heyco Stainless Steel Cable Clamps near the top. Figure 9 shows the strain relief boxes that were manufactured out of Aluminum 6061-T6 and then chemically filmed for corrosion protection.

6.2 Fiber Payoff

The process of pulling the optical fibers into the PBT tubing is underway at SSL. During initial testing, we discovered the manufacturer-installed pull cord of the Miniflex PBT tubing was coated with a talcum-like powder. This raised concerns about overall cleanliness and vacuum-compatibility for the fiber anti-reflection coating runs. Preliminary tests of the the PBT tubing inside a thermal vacuum chamber showed high outgassing rates and residual contamination in the chamber. To improve the cleanliness and make the cables vacuum-compatible, a multi-step cleaning plan was followed and proved to be effective at eliminating the contamination source. The Miniflex was cleaned by first blowing the cable with pressurized GN_2 to remove loose powder. Then, the cable was connected to a pump and flushed with de-ionized water. Afterwards, the cable was rinsed with Isopropanol and dried with GN_2. The cable was baked in ambient pressure for 24 hours at 140°C with a continuous GN_2 purge. Finally, the cable was rough-pumped for 24 hours inside a vacuum oven at 50°C. Each PBT cable was labeled with its KPF designator onto a Brady 2HT-250-2-WT-S-2 PermaSleeve heat-shrink label.

The fiber was paid off into the clean PBT tubing utilizing a payoff system designed in-house. The spool of optical fiber was placed onto a shaft connected to a magnetic drag clutch set to 1 lb of drag. Nylon monofilament

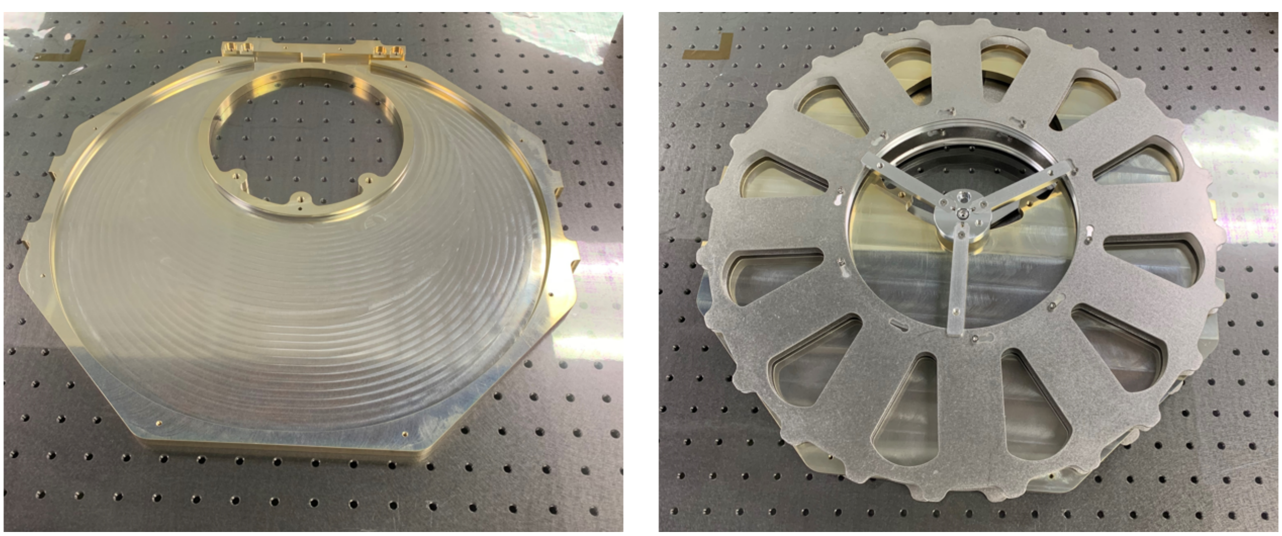

Figure 9. The left image shows the strain relief box for the long optical fibers with a yellow chromate finish (cover plate not shown). The right image shows the spool for the PBT tubing that clamps onto the SRB with a tripod bracket and center fastener.

Downloaded From: https://www.spiedigitallibrary.org/conference-proceedings-of-spie on 02 May 2021
Terms of Use: https://www.spiedigitallibrary.org/terms-of-use

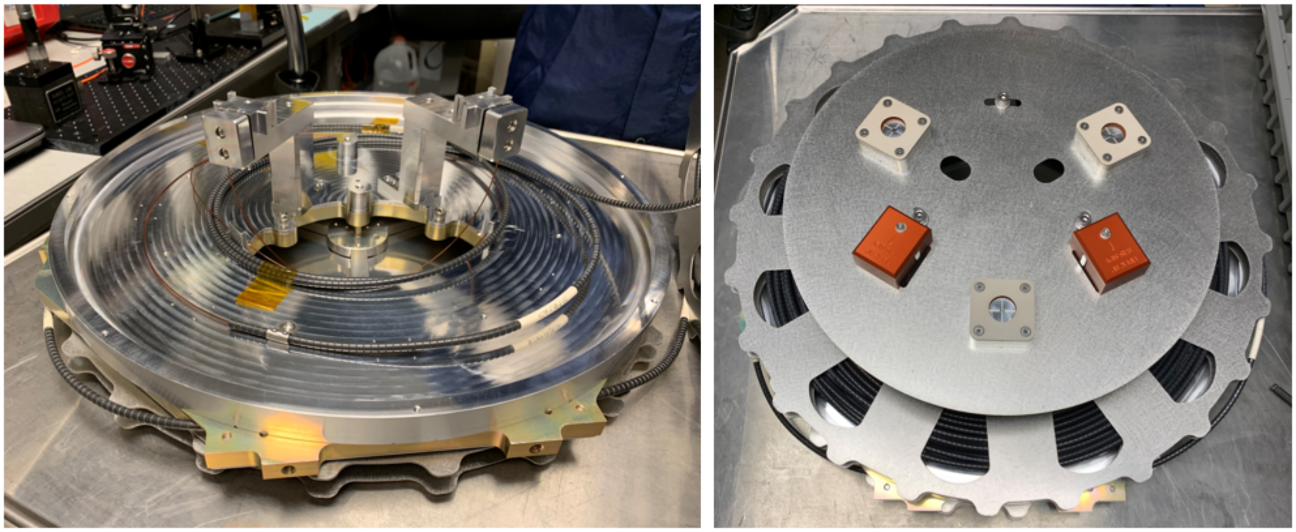

Figure 10. Left: AR coating assembly with the fiber installed into the v-block towers. The inner racetrack provides a nice working surface to secure the loose PBT tubing and fiber before it routes to the v-block tower. Right: The completed AR coating assembly with three optical witness samples and two red-anodized protective fiber caps installed.

was pulled through the PBT tubing and wrapped around a spring-loaded tensioner pulley to compensate for differential rotation rates between the payoff stand and winding spool. The winding spool was driven by a slip-clutch handle with a pre-set force limit of 2.5 lbs, which was under the maximum pull force of 3 lbs determined by the fiber optic maximum tension requirements. After deploying the fiber inside the PBT tubing, a 2 meter long polyimide strain relief tube (from MicroLumen) was installed on each end. This tubing is more flexible and of smaller diameter than the Miniflex, and provides protection to the section of fiber extending beyond the Miniflex tubing. Afterwards, the fiber was loaded onto a custom spool and attached to the strain relief box for storage. At this point the fiber ends were cleaved and then bonded within glass ferrules.

6.3 Fiber Tip Anti-Reflection (AR) Coating

The majority of the KPF fibers will be AR coated, and a mechanical packaging assembly was designed to hold the fibers inside the coating chamber. The AR coating assembly consists of the strain relief box, two spools holding the PBT tubing, a middle racetrack to protect the bare fiber, two posts to hold the ferrulized fiber ends, and a cover plate with optical witness sample canisters. The entire assembly fits within the coating vendor's clearance zone of 18.5 inch diameter and 5.75 inch height. The ferrulized fiber tips were placed inside a v-groove tower and held in place by a sprung block with Viton padding. The AR coating assembly is shown in Figure 10.

7. FIBER SCRAMBLER

Stable illumination of the spectrometer optics is paramount within PRV instruments as any change of the light distribution in either the image or pupil planes can cause displacements of the spectrum that mimic Doppler shifts. One of the primary advantages of using an optical fiber to feed a spectrometer is that it is an effective "scrambler", meaning illumination changes at the fiber entrance (at the telescope focal plane) become smaller and more homogeneous at the fiber output.

We distinguish between the "near-field" illumination pattern, the pattern of light at the fiber tip, and the "far-field" pattern which is the image at a pupil downstream of the fiber tip. Octagonal fibers do an excellent job of scrambling the near-field illumination pattern, both azimuthally and radially; however, the far-field pattern retains a radially non-uniform pattern. This can be mitigated through the use of a double-fiber scrambler system,[10] which swaps the near- and far-fields of the fiber output (Figure 11). The scrambler output is then injected into a second fiber, which in turn scrambles what was originally the far field of the first fiber. The output of the second fiber then displays homogeneous near- and far-field intensity patterns.

Downloaded From: https://www.spiedigitallibrary.org/conference-proceedings-of-spie on 02 May 2021
Terms of Use: https://www.spiedigitallibrary.org/terms-of-use

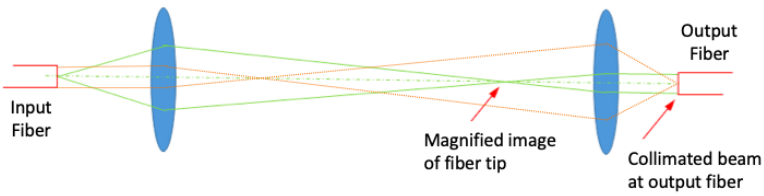

Figure 11. Schematic of the scrambler optical design. The optical system is analogous to that of a microscope. As shown by the green raypath, the first lens forms a magnified image of the fiber tip. The second lens acts as an eyepiece and collimates the beam with a diameter equal to that of the fiber. Hence the near-field becomes a far-field. The red raypath illustrates the symmetry of the design, and how the far-field of the first fiber becomes the near-field of the second fiber.

The "twin-lens" scrambler design employed by KPF is shown in Figure 12. As shown, a vacuum window is placed within the air space between the two lenses, allowing the scrambler to also act as an optical feedthrough at the spectrometer vacuum chamber wall.[11] The KPF design uses this optical scrambler design for three light paths entering the spectrometer vacuum chamber (science, sky and simultaneous calibration fibers), as well as for the exposure meter light path exiting the chamber. While the exposure meter path does not require scrambling, utilizing a scrambler for the feedthrough allowed two similar scrambler systems to be developed with two fibers each. Note the spacing between the scrambler lenses changes with the sizes of the fibers used, however this is accommodated by the scrambler opto-mechanical design.

A prototype scrambler system was designed, built and tested before the KPF PDR. While the system performed well optically, its use in the lab highlighted some shortcomings of the mechanical design. For example, within the prototype design magnets were used to constrain the v-groove blocks holding the fiber ends; this arrangement proved to be indeterminate and led to unrepeatable fiber positions upon removal and replacement. The PDR design was also difficult to work with due to the cylindrical housing with narrow view ports. Overall, the new scrambler mechanical design contains the same optical design and premise of operation, but offers improved functionality.

The new scrambler design can be configured in an open-concept manner to allow plenty of space during alignment. As shown in Figures 13 and 14, an enclosure box is placed around the air-side optics to create a light-tight seal. The expanded PVC sheets are easily removable from the enclosure for routine servicing. On

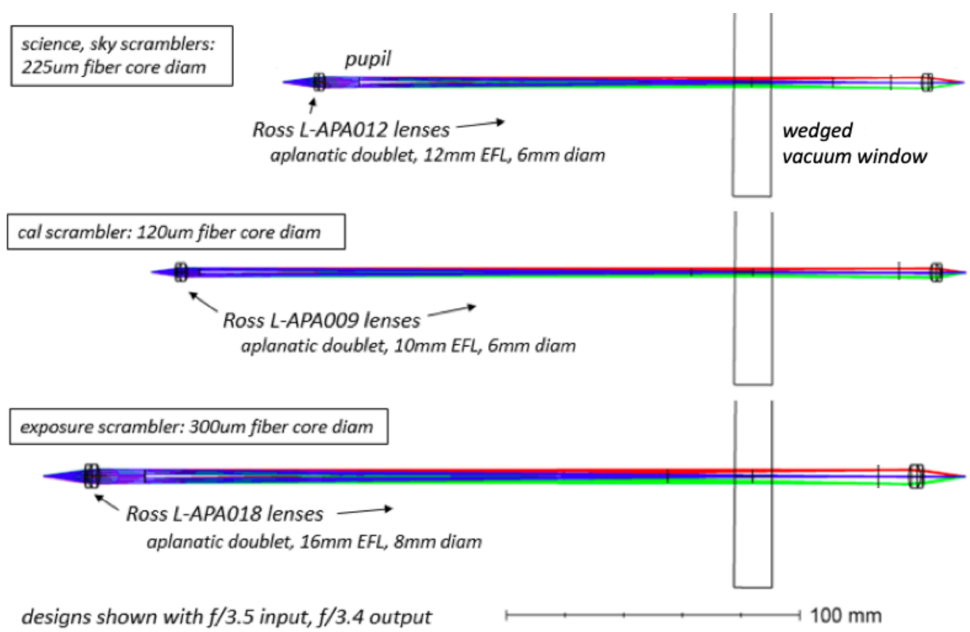

Figure 12. Zemax layouts of the three different scrambler designs used within KPF.

Downloaded From: https://www.spiedigitallibrary.org/conference-proceedings-of-spie on 02 May 2021
Terms of Use: https://www.spiedigitallibrary.org/terms-of-use

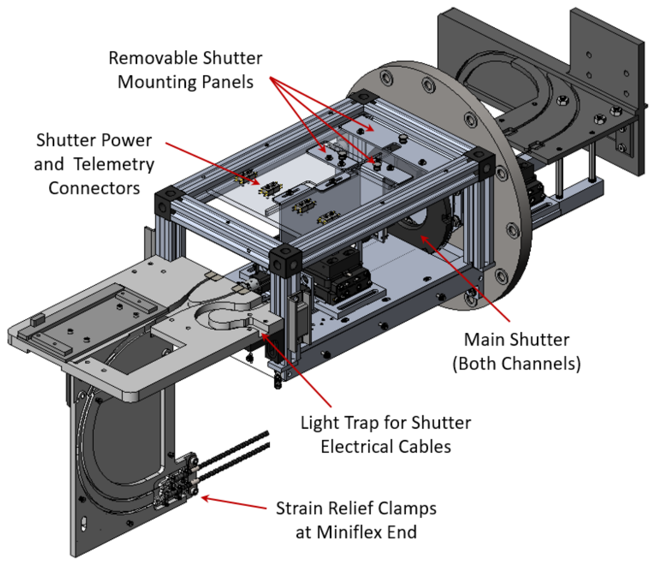

Figure 13. Isometric view of the KPF fiber scrambler fully enclosed. The air-side (front half) of the scrambler has a light-tight enclosure constructed from aluminum extrusion. The extensions at either end are 'racetracks' to constrain and protect the input and exit fibers. External panels on the enclosure and racetracks have been removed or made transparent for clarity.

both sides of the scrambler, black Acetal racetracks route the fiber to the fiber mount. Poron foam is used at the edges to cushion the fiber and seal any gaps. Uniblitz bi-stable shutters are implemented on the science and sky fiber arms to control which arm illuminates the instrument. The main spectrometer shutter (Uniblitz NSS65B) sits in front of the 0.5°-wedged vacuum window. All shutters are mounted on removable panels to simplify maintenance and replacement. A middle baffle is placed between the two fiber channels to prevent cross talk and help suppress stray light.

The individual lens assemblies for the scrambler are shown in Figure 15. The ferrulized fiber sits on a v-groove block that is mounted to a Thorlabs PY005 5-axis stage. This provides sufficient degrees of freedom to align each fiber. A sprung plate with a Viton pad holds the fiber within the v-block. A compact lens assembly sits in front of each fiber. The lens mount utilizes precision ground ceramic balls in the front to establish coplanarity between the lens and housing. Sprung PEEK retainers contact the lens on the top edge and back face to hold the lens in place against the registration features.

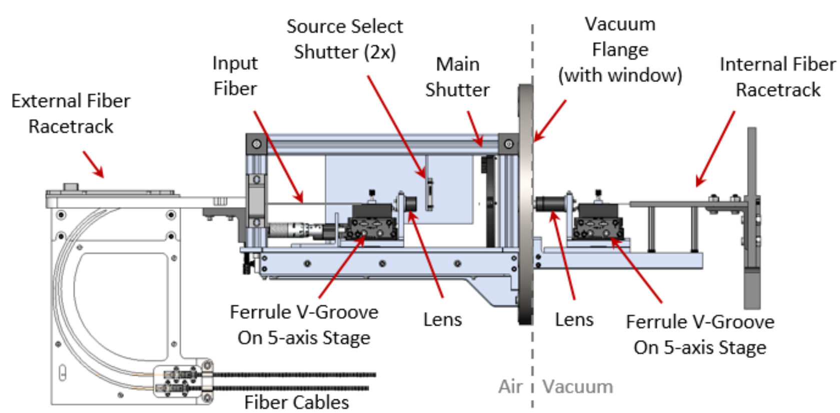

Figure 14. Cross section view of the KPF fiber scrambler which is integrated onto an ISO vacuum flange. External cover panels have been removed or made transparent for clarity.

Downloaded From: https://www.spiedigitallibrary.org/conference-proceedings-of-spie on 02 May 2021
Terms of Use: https://www.spiedigitallibrary.org/terms-of-use

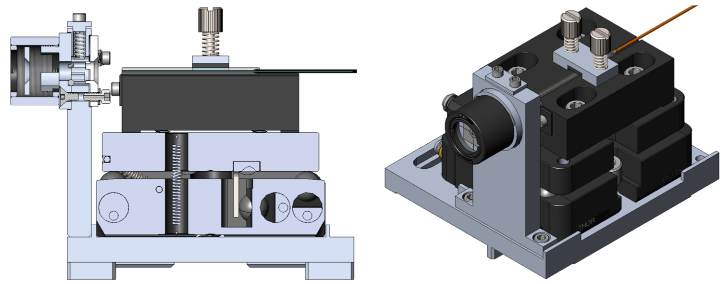

Figure 15. Scrambler lens assembly shown in a cross section view (left) and isometric view (right).

8. VPH TESTING RESULTS

8.1 KPF VPH Overview

As described within Section 2, the main spectrometer employs VPH-based grisms for cross-dispersion. In order provide sufficient cross dispersion, the green channel VPH grating was produced with a line density of 800 lines per mm and the red channel VPH with 450 lines per mm. A summary of the KPF VPH grating requirements are shown below in Table 1. Both gratings were produced by Kaiser Optical Systems (KOSI) and delivered in Q4 of 2019.

Table 1. KPF VPH Grating Specifications and Requirements for Unpolarized Incidence.

Specification	**Green Channel**	**Red Channel**
Wavelength Range	445-600 nm	600-870 nm
Fringe Frequency	810 $\pm$2 l/mm	450 $\pm$2 l/mm
Clear Aperture	204 mm diameter	200 mm diameter
Central Incidence α_0	-30.5°	-24.4°
Substrate	230 mm square, 20 mm thick Fused Silica	

8.2 VPH Efficiency Test Overview

A preliminary set of diffraction efficiency measurements was conducted by KOSI at a few locations across the clear aperture for each KPF grating. These data were re-measured and confirmed at SSL in Q1 2020 using the measurement test equipment and procedures developed by the DESI project.[12] The DESI-developed measurement rig provides automated test sequences to: 1) determine the optimum grating incidence angle and 2) measure the diffraction efficiency at multiple points across the clear aperture of the grating. The measurement rig is shown below in Figure 16. The rig was modified for KPF to accommodate a larger grating (new mount and linear adjustment stage) as well as the use of a monochromator as the input source for the test. The Python automation script was also improved and optimized, based on lessons learned from the DESI measurement campaign.

As can be seen, the measurement rig is a set of linear and rotary actuators that manipulate the grating, as well as the input source and reference detector. The input source consisted of a JY-Horiba Triax 320 monochromator fed with an NKT Photonics Whitelase Micro supercontinuum source. All measurements were done with a monchromator slit width corresponding to a spectral resolution of 1.8 nm FWHM. The output of the monochromator was focused onto a 200 μm, 2m long multi-mode optical fiber whose output was coupled to an off-axis reflective collimator. This produced a collimated beam diameter of 8 mm at the grating, slightly smaller than the reference detector's 10 mm diameter entrance aperture.

Each grating was measured first for its optimum angle of incidence (AOI). This was accomplished by performing a wavelength scan at 5 nm steps across the grating passband, with the beam positioned at the center of the grating. This data was taken at the design AOI (see Table 1), as well as +/- 0.5° and +/- 1° from the design central incidence to cover the full range of adjustment within the spectrometer. Once the optimum AOI was determined, a polarizing beamsplitter was installed on the output of the source. This allowed us to measure

Downloaded From: https://www.spiedigitallibrary.org/conference-proceedings-of-spie on 02 May 2021
Terms of Use: https://www.spiedigitallibrary.org/terms-of-use

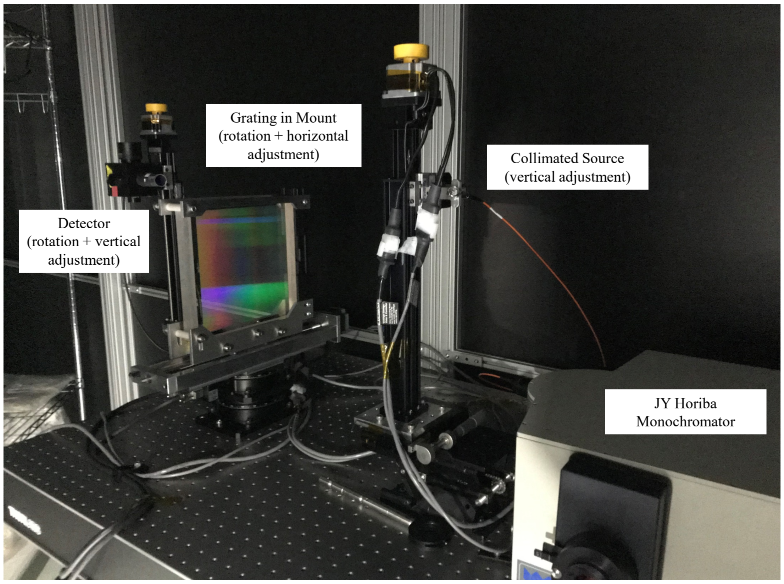

Figure 16. KPF VPH grating under test.

both the P-polarization (beamsplitter in) and average (beamsplitter out) Fresnel reflection components from the front surface of the VPH substrate. This confirmed that: 1) light from the source was unpolarized and 2) the Fresnel reflection component could be properly accounted for in the diffraction efficiency measurement.

Following determination of each grating's optimum AOI, wavelength scans were performed at 96 points across the clear aperture of the grating to determine the uniformity of the grating's diffraction efficiency. These 96 points were sampled at approximately 10 mm steps across the surface of the grating, in a cruciform and X-pattern as shown in Figure 17.

8.3 Efficiency Test Results

Overall, we were able to confirm KOSI's measurements and saw a slight (2-4%) increase in diffraction efficiency. The optimum AOI for each grating were both chosen away from their design AOI due to gains in diffraction efficiency at the "blue" end (green grating) and "red" end (red grating) of the KPF passband. For the green grating, we chose an AOI of -29.5° which increased the overall band average efficiency from 86.4% to 87.7%. This

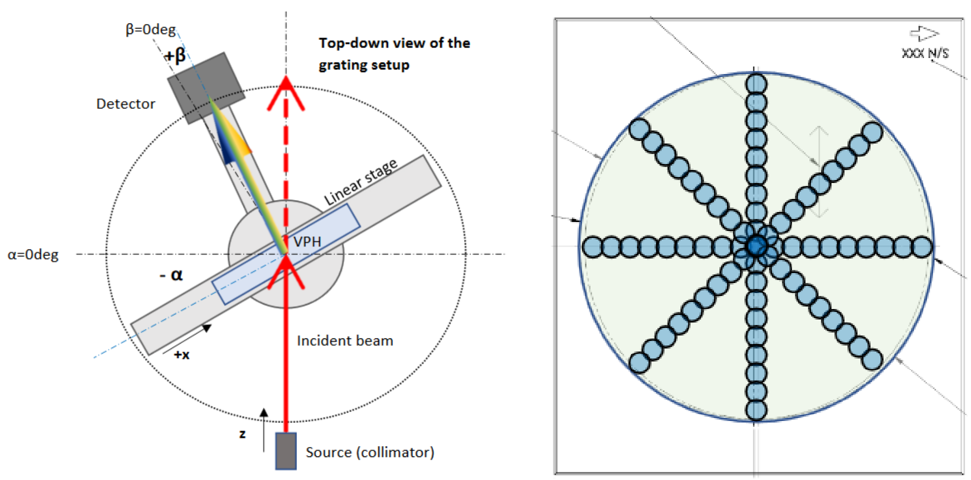

Figure 17. VPH test overview schematic (left) and regions tested under the full grating scan (right).

Downloaded From: https://www.spiedigitallibrary.org/conference-proceedings-of-spie on 02 May 2021
Terms of Use: https://www.spiedigitallibrary.org/terms-of-use

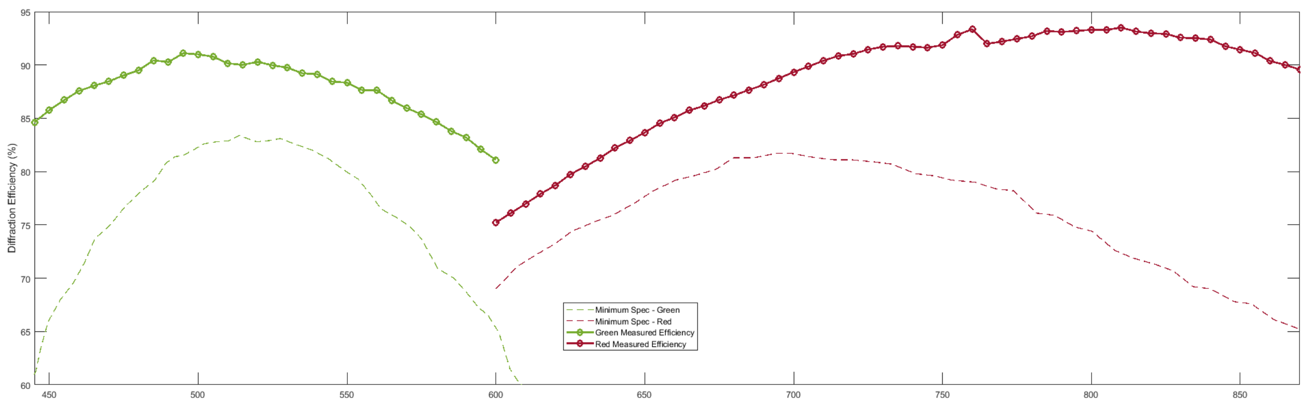

Figure 18. KPF VPH diffraction efficiency measured at SSL far exceeds the production minimum specifications supplied by KOSI.

increased the blue end efficiency from 77.6% to 84.6%. For the red grating, we chose an AOI of -25.4° which slightly increased the overall band average efficiency from 87.7% to 88.6%. This increased the red end efficiency from 82.7% to 89.6%.

Figure 18 shows the measured efficiency of the two KPF VPH gratings over the spectrometer's passband. With the changing of the AOI in each grating, we've seen significant gains (approximately 25%) in diffraction efficiency vs. the production minimum specification at both ends of the spectrometer passband. Overall these gratings exceeded our production minimum specification by ≥5% across at all wavelengths with the noted gains at the "blue" and "red" ends of the KPF spectrometer passband.

9. EXPOSURE METER

An accurate measurement of the time of the flux-weighted midpoint of each exposure is essential to correct for the barycentric velocity of the Earth. During an exposure, a small fraction of the light within the spectrometer is diverted to a separate, low-resolution spectrometer that records the flux time series for all wavelengths across the main spectrometer bandpass. This system accurately tracks the photon arrival times in the parent spectrometer, allowing for precise determination of flux-weighted exposure mid-points as a function of wavelength.

The optical design of the exposure meter has changed slightly since the 2018 KPF paper,[1] although it remains a prism-based spectrometer with a resolving power of approximately 100. The exposure meter accepts light from two fibers; one collecting light from the otherwise unused outboard slices of the science fiber at the spectrometer reformatter entrance, and a sky fiber from the fiber injection unit on the telescope. The optical design is shown in Figure 19.

The exposure meter requires a slit to be applied to both fiber sources, and the addition of an input relay to the design has greatly simplified this requirement. With the slit now in free space (and not bonded-to or otherwise applied to both fiber ends), the two source fibers become completely independent. This has practical advantages for fiber cable fabrication and installation.

As shown in Figure 19, the input relay employs off-the-shelf lenses from Edmund Optics. Of note is that while the relay collimator focal length is set by the f/3.5 f/cone leaving the fiber, the f/# at the slit is an open design variable. Easing the f/# at the slit to f/7 allowed for improved image quality within the system without changing any fundamental spectrometer parameters (magnification, sampling, etc.). This was possible because the lenses on either side of the slit are symmetric and have collimated entrance and exit beams.

Within the exposure meter design, the detector is yawed with respect to the camera axis, allowing correction for focus shift with wavelength. This is a relatively common technique which eases the color correction required of the camera optical design. The exposure meter was originally expected to employ an OTS C-mount lens for the camera, and a Zemax black-box design was obtained from the manufacturer. However, during the opto-mechanical design process it was found that the Zemax black-box dimensions did not match the physical

Downloaded From: https://www.spiedigitallibrary.org/conference-proceedings-of-spie on 02 May 2021
Terms of Use: https://www.spiedigitallibrary.org/terms-of-use

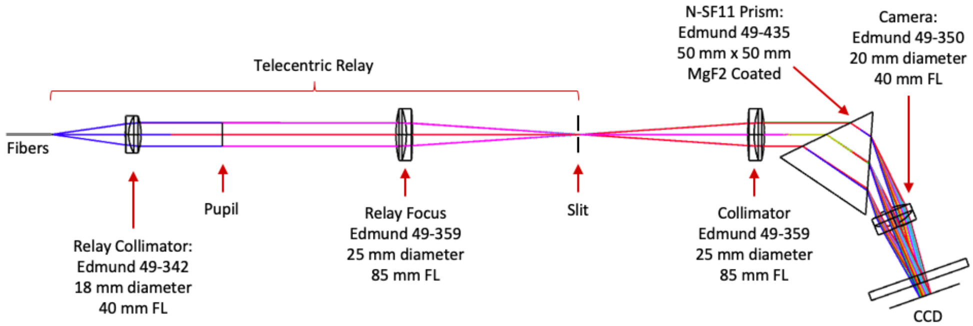

Figure 19. The optical design of the KPF exposure meter. Light enters the instrument from the left via two optical fibers. The system employs a 12 mm collimated beam diameter, which was set by available off-the-shelf prism sizes.

dimensions of the camera barrel. This resulted a collision between the camera and the CCD window owing to the required detector yaw (2 degrees). Given all C-mount cameras have a common back-focus distance for interchangeability, we had to abandon OTS C-mount camera lens designs. Fortunately, as shown in Figure 19, an Edmund Optics doublet lens was found to give acceptable image quality and offer more than enough back-focus to accommodate the detector yaw.

During assembly and initial tests, a ghost spectrum was found within the system. The prism employed has three polished sides, and a ghost path was set up within the prism as shown in Figure 20. This ghost was of relatively high intensity given it was caused by three reflections within the prism itself. It was also in focus as the ghost reflections occurred within a collimated beam. Fortunately this ghost was easily mitigated by the application of a piece of black Kapton tape to the base of prism, which frustrated the reflection at that face.

Figure 21 shows the opto-mechanical design of the exposure meter. Thorlabs cage-system components were used for the input relay optics, with an Edmund Optics mount employed to hold the prism. A custom mount was designed for the camera and detector components. This included a small Thorlabs translation stage to enable camera focus. For detector yaw, the CCD is mounted on a plate that can be rotated with respect to a fixed baseplate. The rotation axis of the upper plate is set by a bullet-nose pin and sleeve system whose axis is co-planar with the CCD front face. This allows for independent adjustments of detector yaw and of camera focus. Both camera focus and yaw are actuated by micrometers, providing precise and repeatable adjustments.

The exposure meter was assembled and aligned at SSL in Q3 of 2020 (Figure 22 shows the assembled system). The opto-mechanical design allowed us to first align the focus-sensitive components separately prior integrating all of the elements onto the breadboard. For all of the laboratory testing, a 300 μm (10 m long) multi-mode optical fiber patch cable was used as the input to the exposure meter. An alignment telescope was employed to align and focus the input fiber first to the relay collimator, then separately used to align the relay focus, slit, and 2nd collimator. Once these elements were aligned and properly focused, they were integrated with the cage-system and positioned with respect to the prism with the use of a mechanical alignment jig. Finally, the CCD and camera lens were installed behind the prism with the use of the same mechanical alignment jig.

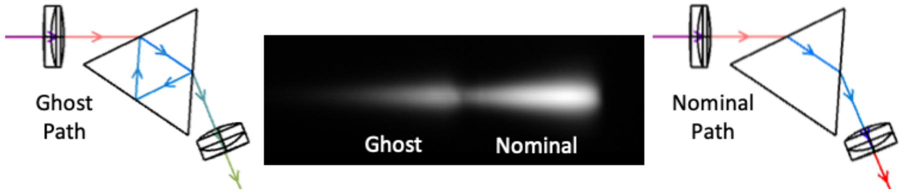

Figure 20. Preliminary laboratory spectra (as shown here at center for a single fiber with a tungsten-halogen source) displayed a strong ghost spectrum adjacent to the nominal spectrum. Non-sequential Zemax raytraces (left and right of center) showed the cause of the ghost to be internal reflections within the prism.

Downloaded From: https://www.spiedigitallibrary.org/conference-proceedings-of-spie on 02 May 2021
Terms of Use: https://www.spiedigitallibrary.org/terms-of-use

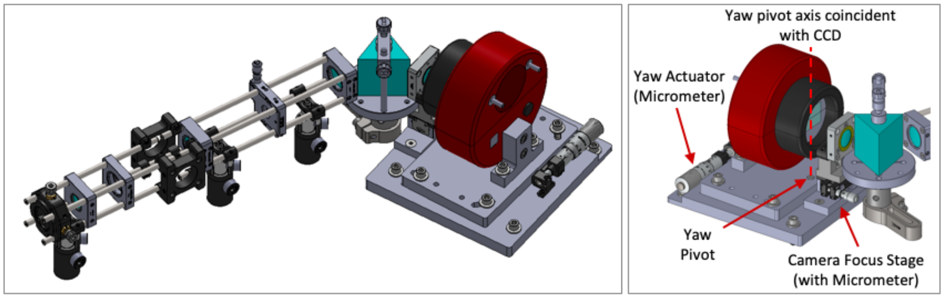

Figure 21. Opto-mechanical design of the exposure meter. The system mounts on a 12” x 24” x 0.5”-thick aluminum breadboard. The detector shown is an ATIK 11000 which was used for preliminary testing.

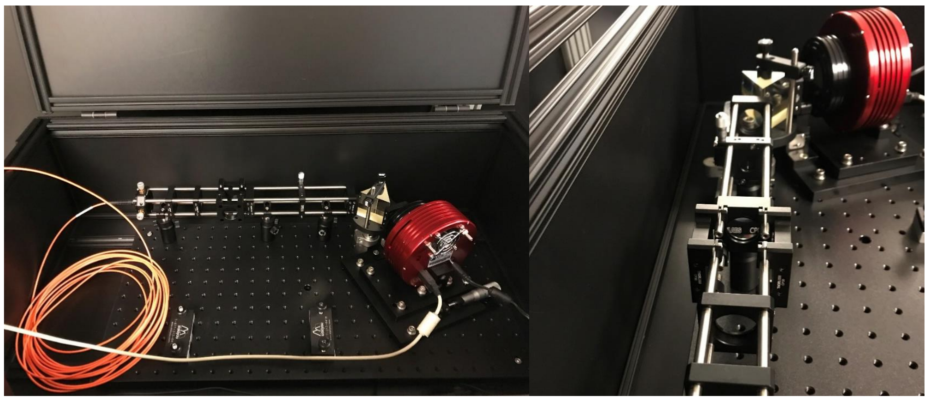

Figure 22. The KPF exposure meter undergoing testing in the laboratory. The system sits within a protective enclosure, shown here with the hinged lid opened. The detector is an ATIK 11000 which was used for preliminary testing.

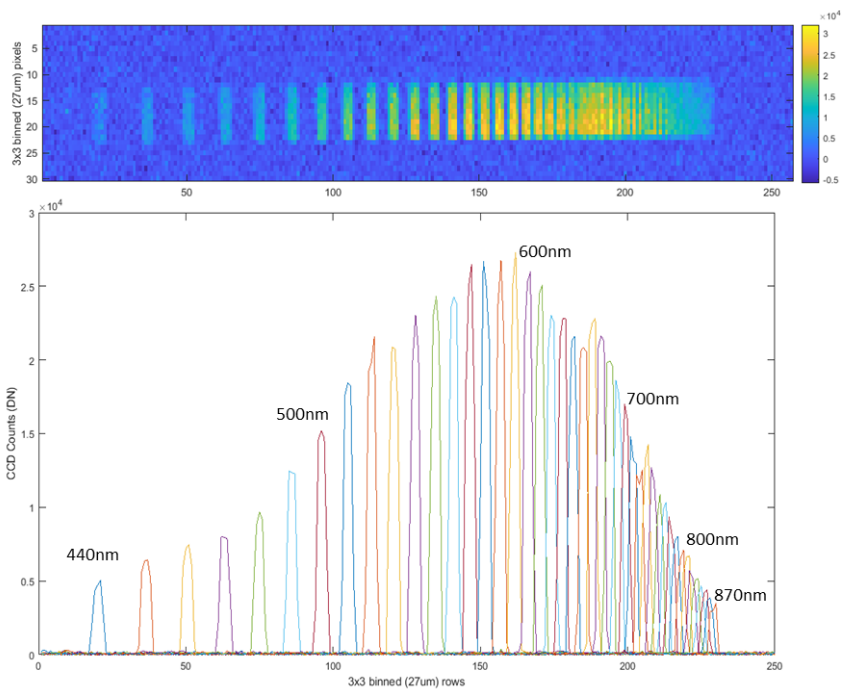

Figure 23. Co-added image of a KPF exposure meter wavelength scan across the main spectrometer bandpass in 10 nm steps (above), and corresponding row profile at each wavelength step (below). Note these images were taken with the same CCD exposure time, and the fall-off in counts red-ward of 600 nm is due to the fall-off in the ATIK 11000 CCD quantum efficiency.

Downloaded From: https://www.spiedigitallibrary.org/conference-proceedings-of-spie on 02 May 2021
Terms of Use: https://www.spiedigitallibrary.org/terms-of-use

After mechanical assembly, the input fiber was coupled to a JY Horiba Triax 320 monochromator (the same used for the VPH grating tests and discussed in Section 8.2). The monochromator was employed to evaluate the image quality of the exposure meter as a function of wavelength with only a single resolution element. This also allowed us to determine a preliminary wavelength solution for the spectrometer. Figure 23 shows the results of the preliminary wavelength solution and image quality of the exposure meter. Overall, the exposure meter meets its requirements for image quality across the passband. The team is performing a final trade study on detector selection before proceeding with the final laboratory tests with the chosen detector in place.

ACKNOWLEDGMENTS

The authors thank the Heising-Simons Foundation, the National Science Foundation (award 2034278 through the Mid-Scale Innovations Program in Astronomical Sciences), private donors, the W.M. Keck Foundation, the University of California, Berkeley, the California Institute of Technology, the University of Hawaii, the Jet Propulsion Laboratory, and the Mt. Cuba Astronomical Foundation for financial support of KPF. The authors also wish to thank Winlight Systems for their valuable contributions to the designs of the reformatter and cameras, as well as the DESI project for sharing their camera designs and their expertise with optical fibers.

REFERENCES

[1] Gibson, S. R. et al., "Keck Planet Finder: Preliminary Design," in [*Ground-based and Airborne Instrumentation for Astronomy VII*], Evans, C. J., Simard, L., and Takami, H., eds., **10702**, 1778 – 1797, International Society for Optics and Photonics, SPIE (2018).

[2] Probst, R. A. et al., "A laser frequency comb featuring sub-cm/s precision for routine operation on HARPS," in [*Ground-based and Airborne Instrumentation for Astronomy V*], Ramsay, S. K., McLean, I. S., and Takami, H., eds., *Society of Photo-Optical Instrumentation Engineers (SPIE) Conference Series* **9147**, 91471C (July 2014).

[3] Collier Cameron, A. et al., "Three years of Sun-as-a-star radial-velocity observations on the approach to solar minimum," *MNRAS* **487**, 1082–1100 (July 2019).

[4] McBride, D. and Hudek, S., "Etching zerodur with hydrofluoric acid vs. ammonium biflouride, KOTN-579," tech. rep., W.M. Keck Observatory (2011).

[5] Wright, J. T. and Robertson, P., "The Third Workshop on Extremely Precise Radial Velocities: The New Instruments," *Research Notes of the American Astronomical Society* **1**, 51 (Dec. 2017).

[6] Roy, A. et al., "Scrambling and modal noise mitigation in the Habitable Zone Planet Finder fiber feed," in [*Ground-based and Airborne Instrumentation for Astronomy V*], *Proc. SPIE* **9147**, 91476B (July 2014).

[7] Sirk, M. M. et al., "An optical fiber double scrambler and mechanical agitator system for the Keck Planet Finder spectrograph," *Proc. SPIE* **10702** (Aug. 2018).

[8] Petersburg, R. R. et al., "Modal noise mitigation through fiber agitation for fiber-fed radial velocity spectrographs," *The Astrophysical Journal* **853**, 181 (Feb 2018).

[9] Sirk, M. M. et al., "The Fiber Agitator System for the Keck Planet Finder Spectrograph (in prep)," (2021).

[10] Hunter, T. R. and Ramsey, L. W., "Scrambling properties of optical fibers and the performance of a double scrambler," *PASP* **104**, 1244–1251 (Dec. 1992).

[11] Avila, G. et al., "Performances of HARPS and FEROS fibers in La Silla ESO Observatory," in [*Ground-based Instrumentation for Astronomy*], *Proc. SPIE* **5492**, 669–676 (Sept. 2004).

[12] Ishikawa, Y. et al., "Comprehensive measurements of the volume-phase holographic gratings for the Dark Energy Spectroscopic Instrument," *The Astrophysical Journal* **869**, 24 (Dec. 2018).

Downloaded From: https://www.spiedigitallibrary.org/conference-proceedings-of-spie on 02 May 2021
Terms of Use: https://www.spiedigitallibrary.org/terms-of-use